Axonal Spectrum Imaging (AxSI): In-Vivo mapping of axonal diameter distributions in the human brain

Hila Gast (gast.hila@gmail.com)
Tel Aviv University
Assaf Horowitz
Tel Aviv University
Ronnie Krupnik
Tel Aviv University
Daniel Barazany
Tel Aviv University
Shlomi Lifshits
Tel Aviv University
Shani Ben-Amitay
Tel Aviv University
Yaniv Assaf
Tel Aviv University

Article

Keywords:

Posted Date: July 15th, 2022

DOI: https://doi.org/10.21203/rs.3.rs-1835012/v1

Abstract

In this paper we demonstrate a generalized and simplified pipeline called axonal spectrum imaging (AxSI) for *in-vivo* estimation of axonal characteristics in the human brain. Whole-brain estimation of the axon diameter, *in-vivo* and *non-invasively*, across all fiber systems will allow exploring uncharted aspect of brain structure and function relations. While axon diameter mapping is important in and of itself, its correlation with conduction velocity will allow, for the first time, the explorations of information transfer mechanisms within the brain. We demonstrate various well-known aspects of axonal morphometry (e.g., the corpus callosum axon diameter variation) as well as other aspects that are less explored (e.g., axon diameter-based separation of the superior longitudinal fascicules into segments). Moreover, we have created an MNI based mean axon diameter maps over the entire brain for a large cohort of subjects providing the reference basis for future studies exploring relation between axon properties, brain function, physiology and behavior.

Introduction

The ability to measure physiological features of the nervous system in humans is limited. Classical approaches such as single unit recording, electrocorticographics (eCog) or local field potentials can be measured in humans invasively when aligned with other clinical needs [1, 2]. The investigation of healthy brain neurophysiology is therefore confounded to non-invasive techniques such as evoked potentials (via EEG) and functional imaging (via BOLD fMRI or fNIRS) [3]. While these methods affected tremendously our knowledge on the functioning human brain, each one lacks important features such as temporal or spatial resolution, as well as specificity. Consequently, when diffusion MRI was shown to be sensitive to axonal morphology, it potentially provided an opportunity to explore, for the first time, *in-vivo* and non-invasively, one of the most basic physiological features of the brain - the conduction velocity (as conduction velocity was shown to be correlated with axon diameter in [4–7]).

The Diffusion MRI signal has been shown to be sensitive to axon diameter under unique experimental conditions [8–11]. Several biophysical models were developed to estimate the axonal diameter distribution from the diffusion MRI signal: the first was AxCaliber, followed by ActiveAx, AxCaliber3D, ActiveAxADD, Commit, Amico, and other, unnamed, methods [12–20]. These models demonstrated their usefulness for several distinct tracts/bundles mainly focusing on the corpus callosum. This sensitivity towards axon diameter was validated versus the state-of-the-art histology (electron microscopy) [8, 18, 21, 22]. While first indications of diffusion MRI sensitivity towards axon diameter appeared to be very promising, following works raised concerns regarding the sensitivity, specificity, and suitability of this approach for exploring axon diameters in a clinical setup.

The ability to infer information of axon diameter is embedded in the assumption that diffusion within axons is restricted while elsewhere it is free or hindered. In an axon diameter sensitive diffusion MRI experiment, we need to favor the contribution of restricted diffusion over other modes diffusion [9, 23, 24]. This might be achieved by tuning of the experimental parameters (i.e., the diffusion times (Δ) and diffusion weighting (b-value)) [25–28].

Several studies challenged the assumed sensitivity, specificity and selectivity of restricted diffusion towards intra-axonal water [29, 30]. While they may point to valid concerns, experimental evidences suggest that the contribution of intra-axonal water to restricted diffusion signal dominates other factors (see supplementary material, section A) [25–28, 31–34] leading to the following conclusions:

1. Myelin causes significant restricted diffusion in neuronal tissue.
2. Diffusion experiments at high b-values are selective and specific to restricted diffusion water pools.
3. Intra-axonal water is the main source of restricted diffusion water population in neuronal tissue.

These evidences were the basis for axon diameter estimation frameworks (as listed above). In all these frameworks, the tissue is modeled as a combination of hindered and free diffusion in the extra-axonal space and diffusion within impermeable cylinders to represent the intra-axonal space. The models differ in their estimation of fiber orientation dispersion, exchange rates between the modeled compartments, as well as in the analytical description of diffusion within cylinders.

Assuming that certain experimental conditions indeed favor intra-axonal water signal, other critiques were raised whether these experimental conditions can be met in a clinical MRI setup [19, 29, 35] or even infeasible at all [36]. However, experiments designed to tackle these concerns suggested that they are not as severe as suspected (see Supplementary material, section B). Noteworthy and most important is the invariance of the signal decay to the gradient duration when measured *in-vivo*. This invariance paves the path to a potential suitability of clinical scanners to axon diameter estimation through diffusion imaging. Moreover, it also greatly simplifies the modelling approach leading to an easy to implement and robust modeling framework termed AxSI.

The AxSI (Axonal Spectrum Imaging) framework, introduced in this paper, suggests a simplified approach to estimate axon diameter distribution per reconstructed axonal fiber or fascicle streamline (see Methods) dealing with all of the abovementioned concerns. Validation of this method on rodent data (see Supplementary material, section C) indicates the high applicability and suitability of this method to a clinical MRI setup. It must be noted that the accurate, exact, and absolute calculation of the axon diameter is most likely unachievable, yet we claim that AxSI provides the best proxy of axon diameter information for the reasons listed above. We demonstrate the outcome of this generalized framework for the estimation of axon diameter properties of several fiber systems in the human brain, including but not restricted to the corpus callosum. We further show the utility of using AxSI for estimating ADD over a large database of diffusion MRI measurements serving as a reference base for future studies on conduction velocity and brain function and behavior.

AxSI Modeling Framework:

In this paper we suggest a framework for estimating axonal diameter distributions, per extracted fiber streamline, called axonal spectrum imaging (AxSI). AxSI uses several experimental considerations that simplify both acquisition and modeling algorithms on one hand and overfitting by many free parameters on the other hand.

AxSI follows the same general description of AxCaliber (and other frameworks) that suggest that the measured signal is a linear combination of three water pools [37, 38]: CSF water, hindered diffusion (cellular and extracellular) and restricted diffusion (axonal). To simplify the modeling approach, first assumption of the model is that there is no exchange between axonal and extra-axonal diffusion (despite experimental evidence that suggests exchange is apparent to some extent, see supplementary material, section B). In addition, we assume that; free diffusion occurs within the CSF compartment (described as Gaussian diffusion), hindered diffusion (described as diffusion tensor) occurs within the extra-axonal compartment, and restricted diffusion occurs within the intra-axonal compartment (further described by motion within impermeable cylinders, [38]) (Eq. 1). This is the second assumption of the model, although it is plausible that restricted diffusion also occurs to some extent in the extra-axonal space.

$$E(b,\Delta) = A_f \bullet E_f + A_h \bullet E_h + A_r \bullet E_r \text{ [1]}$$

Where:

- $E(b,\Delta)$ is the observed signal decay (Δ is the diffusion time, and b is the diffusion weighting)
- A and E represent the volume factions and signal decays of the three compartments (respectively): free diffusion (*f*), hindered diffusion (*h*), and restricted diffusion (noted by *r*).

In AxSI, common diffusion indices (e.g. mean diffusivity in the hindered space) as well as fiber orientations are estimated separately by conventional procedures [39]. As such, the modeling of E_f and E_h is done separately and taken as priors (predictors) for compartment population estimations (see library-based analysis below). Yet, the most complicated and controversial modeling of any axon diameter estimation framework is the restricted diffusion component, which is presumed to represent intra-axonal water. AxSI takes advantage of the *in-vivo* insensitivity of the measured signal to the gradient pulse duration (δ), which is a key factor in modeling strategy decisions (see supplementary material, sections B and C). This insensitivity allows to use a simple relation between the measured signal and the axon diameter developed previously for

certain experimental conditions [40]. As the *in-vivo* measured signal is insensitive to the experimental conditions (δ, Δ ; *vide infra*), the use of Eq. 2 to describe diffusion within impermeable cylinders as a proxy to axons appears adequate and feasible:

$E_{ax}(q,R) = E_0 e^{-q^2R^2}$ [2]

Where:

- q is the diffusion weighting factor that incorporates the gradient strength and gradient duration ($q = \gamma\delta g$)
- R is the axon diameter

The simplification of the relation between the measured signal and the axon diameter (Eq. 2) dramatically eases the implementation of the framework for axon diameter estimation. Yet, the novelty of AxSI is the estimation of the axonal diameter distribution (ADD) using a linear fit of the measured signal to a set of predictors (library) that simulate, per pixel, the diffusion MRI signal for a series of predetermined axon diameters that cover the range of possible CNS axon diameter values. This axonal spectrum diffusion MRI signal library, which also includes the E_h and E_{csf} estimation, is fitted to the measured signal to estimate the relative weight or contribution of each axonal predictor to the measured signal as well as the population fractions of the hindered and CSF components.

Critical to the suggested fitting routine is a regularization term (in our case Tikhonov approach) that ensures fitting optimization to a smooth axon distribution function, overcoming the possible overfitting to the noisy and limited number of measured signals as given in Eq. 3:

$E_r(b,\Delta,R) = \Sigma_{k=1}^{k}\pi_k \mathbb{E}\left[E_r(b,\Delta,R_k)\right]$ [3]

Where π_k are the weights for each predictor.

In this case, we can estimate directly π_k using constrained Tikhonov regularization. Once the weights of different diffusion components are computed (in our implementation there are 160 axon diameters), we can compute several maps including axonal volume fraction, mean axon diameter as well as extra-axonal diffusivity. Using conventional fiber tracking, we can compute, per reconstructed streamline, the averaged axon diameter along a path and demonstrate variations in axonal populations across different fascicles (see Methods).

AxSI analysis script is available at: https://github.com/HilaGast/AxSI.git

Results

Axon Diameter Weighted Connectome and Fiber Maps

Using the AxSI framework, we were able to generate three-dimensional brain fiber representations (see Methods) that embed axon diameter information to the extracted fiber tracts.

Figure 1A presents an example of a single subject whole brain representation of streamlines weighted by the average ADD along each streamline. From this representation, network matrices with edges weighted by the average ADD or the number of streamlines was calculated (Fig. 1B and 1C, respectively). Notably is the difference between the streamlines and ADD weighted connectomes (Figs. 1B-C) highlighting different aspects of network properties.

Such maps can visualize and quantify known trends in axon diameter distribution in the brain (e.g., the corpus callosum [41]) and other representations that are less commonly described in the literature. In Fig. 2A a representation of the ADD in the CC of a single subject is demonstrated. A violin plot shows the known trend of smaller ADD values in the Genu and Splenium and larger for the Body parts of the CC, using the AxSI framework, for three different diffusion protocols (Fig. 2E, see details in Methods). Repeated-measures ANOVA resulted in significant differences between different parts of the CC for all three

protocols: $\Delta/\delta = 43.1/10.6_{ms}$; $F(4,68) = 19.9$, $p = 6.7X10^{-11}$, $\Delta/\delta = 60/15.5_{ms}$; $F(4,64) = 4.02$, $p = 5.7X10^{-3}$, $\Delta/\delta = 45/15_{ms}$; $F(4,128) = 15.43$, $p = 2.5X10^{-10}$.

Other tracts also demonstrated patterns and variability in ADD. In Fig. 2A-D, different streamlines are colored according to their estimated mean axon diameter (eMAD), where hot color-scale is used to visualize the different axon diameter (red represents larger axons). It is possible to observe that CST in the middle of CR is salient by its larger axons compared to its surroundings (Fig. 2B) (shown previously in [42]). Moreover, both the SLF and IFOF seem to have several sub-bundles, distinguished from each other by their ADD (Fig. 2C-D).

Axon Diameter Weighted Cortical Surface Representation

A group analysis with AxSI framework on HCP subjects (see Methods), was done to create an axon diameter weighted surface representation. In Fig. 3, each cortical area from the Brainnetome Atlas is weighted by the average value of eMAD of all streamlines entering/exiting it and averaged again for the entire group. It is easy to notice that each brain region is characterized by different axon sizes that connect it to other parts of the brain. Darker colors (darker red) in the figure, represent larger axons.

Averaged Axon Diameter White Matter Reference Map

Finally, we created an average axon diameter WM map, using the group of HCP subjects (see Methods). The maps, created using the AxSI framework, were then registered to MNI space to enable averaging across subjects. The resulting map represents the distribution of estimated axon diameter in the white matter of the healthy human brain young adult. Figure 4 shows highlight slices from this WM atlas (entire dataset is given in Supplementary Fig. S4). For example, in the mid sagittal slice (upper left), the known pattern of ADD in the CC is demonstrated. In a sagittal slice of the left hemisphere (lower left), the CST is salient in red, for having larger axons, as expected. Interesting to note in the axial slice (upper right) the difference in estimated MAD between the anterior and superior limb of the thalamic radiation. Another pattern worth mentioning appears in the WM of the temporal lobe in the coronal slice (lower right). It demonstrates several different bundles, that differ in their eMAD, with blue-purple that represent lower values, for the Fornix (Fimbria)/Stria terminalis, green-yellow represent larger values in the ILF (Inferior Longitudinal Fasciculus) and yellow-orange spot for the IFOF with the largest estimated MAD in this section.

Discussion

The axon diameter is one of several important measures of the nervous system that provide unique insight into the physiology of information transfer in the brain. While traditionally axonal morphometry could have been measured only by invasive histological procedures, the suggested framework in this paper, AxSI, offers a platform for estimating axonal properties in-vivo and non-invasively. Over the last decade it has been repeatedly shown that diffusion imaging is sensitive to axonal size. While the magnitude of this sensitivity is still under debate, it is agreed that certain experimental conditions may favor this unique axonal characterization. Despite the discussion on how to increase the sensitivity of diffusion imaging to axonal properties, the information embedded in axon diameter estimation using MRI is unequivocal.

However, the ability of AxSI to infer axonal properties relies on several assumptions and modeling approaches that must be well understood before using this method routinely. First, as in any model, the obtained parameters are only estimated and not directly measured. The word ‘estimated’ should be further emphasized, as MRI cannot reach the resolution level that allows visualization of axons, but it infers their existence and size based on the characteristics of water diffusion. As described above, water diffusion in neural matter is a complicated process that occurs in several compartments that may share similar diffusion characteristics (diffusion coefficient, hindrance to diffusion, etc.), therefore the biophysical modeling of axon diameter is challenging and may be considered ill-posed. In addition, while validation of AxCaliber/AxSI against the traditional electron microscopy direct measure of axon diameter has been performed, true validation of this measure in-vivo is obviously out of reach. Yet, previous studies have shown that the estimated axon diameters using AxCaliber fit the expected axonal size

variability along the corpus callosum, indicating the sensitivity of this method to known variability [8, 23, 24, 43, 44]. Moreover, correlation with physiological measures, such as conduction velocity, also suggest that this measure of axonal diameter is as physiologically relevant as the traditional electron microscopy measures [7]. Those validations suggest that large population studies are essential to explore new features of brain structure/function relations with AxSI.

Since the first demonstration that diffusion MRI is sensitive to axon diameter over 15 years ago [9], significant limitations and concerns regarding the method have been raised. Additionally, the complicated and somewhat ill-posed modeling framework reduced the applicability of the method to the neuroscientific community. As there are only a few in-vivo markers of brain microstructure properties that have direct physiological meaning, the concerns and obstacles of estimating axonal diameter from MRI should be untangled.

Many papers have dealt with the possible effects of exchange, compartmentalization, and experimental conditions (gradient strength, duration) on the parameters computed from the various frameworks for axon diameter measurement [19, 29, 30, 35, 36, 45–47]. As shown in the supplementary material (section A, B and C), while these effects are meaningful, they cannot completely diminish the observed sensitivity to axon diameter (Fig. S1-3). Taking advantage of some experimental conditions can even favor axon diameter over other factors. As such, the experimental conditions described above provide a diffusion MRI signal that has good specificity and sensitivity to axon diameter.

This experimental optimization still requires a robust and simple modeling framework to increase its applicability and impact. In recent years, the use of machine learning procedures to predict and explain measured signals has become more feasible providing new approaches to estimate free parameters of a model from noisy, sub-sampled data [48–50]. AxSI follows this concept and estimates, per pixel, a set of possible signals that represent different axon diameters. Instead of optimizing the axon diameter directly, AxSI regresses the axon diameter dependent signal library to find the best combination of all possible predictors that explains the measured signal while maintaining smooth weighting distribution function over all possible axon diameters. This approach dramatically simplifies the modeling routine and provides a more robust and stable axon diameter estimation approach.

It should be noted that AxSI, as any other MRI based axon diameter framework, does not directly measure the axon diameter. Rather, it provides a proxy to the diameter via indirect modeling of the diffusion MRI signal. This should not weaken the impact or use of the methodology, since most MRI frameworks suffer from the same indirect interpretation problem: functional MRI does not directly measure brain function but rather susceptibility changes following hemodynamic response to brain activity [3], myelin mapping [51] doesn't measure myelin but rather relaxometry manifestations of myelination, diffusion MRI doesn't measure diffusion but rather displacement (39). Following this jargon, AxSI provides a proxy of the axon diameter, and its extracted indices should be indicated as eMAD or estimated axon diameter distribution (eADD).

In this paper we use AxSI to estimate the MAD and combined it with fiber tracking to visualize tract-specific axonal properties. Each tract shown in Fig. 1–2, was colored according to the mean MAD of the pixels that contribute to the tract (see Methods). Using this visualization procedure, some known neuroanatomical features of axon fascicles become apparent, consequently increasing the validity and impact of the method. For example, the ability to visualize the pattern of axon diameter changes along the corpus callosum (Fig. 2A), highlighting the high MAD in the body of the CC while smaller values in the splenium and genu region, became the hallmark of axon diameter validation [41]. Moreover, the higher MAD values in the cortico-spinal tract compared to other segments of the corona radiata indicate the fast transmission of signal along the motor pathways compared to other fascicles. Noteworthy is the small axon diameter measured at the frontal/temporal transition zone, where the uncinate and inferior fronto-occipital fascicle passes to the frontal lobe, that is in agreement with histological findings [52].

Comparison of AxSI results with histology is limited. First, there is a very limited number of studies measuring axon diameter properties of different fascicles in the human brain [41, 52, 53]. Second, the shrinkage of the tissue in histological preparation underestimates the real axon diameter and probably reduces the variability across fascicles considerably. This stands in contrast to AxSI (and previous methods) that overestimates the axon diameter values. Yet, the above-mentioned observations and comparisons with histology provide sufficient validation to AxSI, thus enabling it to explore other uncharted variations in

axonal properties of different tracts. For example, the two massive long-range connections in the human brain: the inferior fronto-occipital fasciculus (IFOF) and superior longitudinal fasciculus (SLF) appear to have sub segments with different axon diameter properties (see Fig. 2C-D). At least for the SLF, these segments resemble that anatomical separation of the SLF into 3 segments. Still, the relevance of these observations should be tested in future studies that will try to relate reaction time or other behavioral aspects that should be related to these fiber-systems across a large population cohort.

The surface presentation of AxSI indicates a unique view of the cortex colored by the eMAD of fibers that project to it. It appears that large fiber fascicles project more frequently to somatosensory and motor areas, as well as to visual and auditory cortices, while lower axon diameter projects to more frontal and anterior temporal regions, probably indicating slower transmission of information to these regions. Such presentation could be the base for connectome analysis integrating axon diameter properties as weights to the edge strength (Fig. 1B). This might provide a more physiological interpretation of the connectome, rather than more spurious measurements such as number of streamline or mean FA [54, 55].

Lastly, we have computed AxSI on 324 random subjects from the HCP database. From these datasets, we were able to create a mean eMAD map in MNI space, providing a reference quantitative map for future studies (see supplementary material Fig. S5). This map allows to explore anatomically the eMAD property of different areas in the WM of the human brain (computed eMAD map is available at: https://github.com/HilaGast/AxSI.git). Moreover, it might provide the basis of an eMAD-based WM atlas. Such an atlas would define different WM anatomical areas based on their microstructural physiology.

While AxSI framework coped with most concerns that were raised over the years, it is still not free from limitations. Aside from conventional MRI limitations that includes signal to noise and resolution issues that need to be sufficient to achieve accurate eMAD modeling there are additional, more specific to the method, limitations. To achieve high sensitivity towards axon diameter it is required to increase the relative weighting of restricted diffusion water populations [8, 9, 24, 28, 56]. Yet, the ability of a diffusion MRI experiment to be sensitive and accurate to restricted diffusion that occurs in a 5 micron and 0.5 micron axon simultaneously depends, in theory, on the experimental conditions [19, 24]. To be sensitive to small-diameter axons there is a need to apply extremely strong diffusion weighting (high-b values) that is achieved by using the shortest possible period of diffusion tagging (termed δ in diffusion MRI pulse sequence) and high amplitude of diffusion gradients (g). There is no magic number for this sensitivity, some simulations suggest that axons with diameter smaller than 5 microns will be indistinguishable, while others indicate 2 microns as the minimum barrier depending on the experimental conditions [28, 36, 57].

The concerns that have been raised over the years regarding the use of diffusion MRI for measuring or estimating axon diameter properties are indeed troubling and hold back the potential uses of this method in neuroscience. All the concerns raised previously (summarized in the introduction and supplementary material) are a result of modeling and simulations and thus, as long as the mathematical description of the diffusion signal is correct, these concerns are valid [45]. However, diffusion MRI is a complicated method to be modeled: First, it measures a stochastic phenomenon; the random motion of water molecules, even for the case of water diffusion within a glass requires several assumptions [58]. Second, the effects of membranes as restrictive or semi-permeable barriers are unknown and hence can only be speculated [59–61]. Third, the ground truth for any axon diameter estimation is histology which may considerably differ from in-vivo conditions [62]. This complexity cannot be resolved by including all possible water pools, biophysical properties (e.g., exchange), and experimental conditions.

Yet, despite the validity and significance of the limitations, none of them, to our understanding, can overrule the sensitivity of diffusion MRI, at specific experimental conditions, to axonal morphometry.

Summary

The rationale for developing the AxSI framework was to provide the neuroscience community with tools to estimate this property in-vivo. Modeling conduction velocity and information transfer are one of the holy grails of neuroscience and AxSI provides a robust and simple platform to achieve that. The new opportunity to explore the fine morphometry of axons and neural processes provides the ability to investigate brain anatomy in-vivo over large population cohorts which may reveal, for

the first time, the role of axons in various conditions. As a result, the role of axons and axonal size in disease may be determined and studied in depth. It is reasonably hypothesized that axonal morphometry can serve as a mirror for normal brain development and may provide the neuroscientist, the neurologist, or neuropsychiatrist with better tools to explore brain physiology.

Materials And Methods

Data

60 human subjects were healthy adults scanned as part of the Tel Aviv University (TAU) Strauss Neuroplasticity Brain Bank, and the imaging protocol included additional sequences that were not used in this study. They were scanned using either diffusion protocol 1 (23 subjects: 12 females, age 19–46 years, mean 26.8) or diffusion protocol 2 (37 subjects: 19 females, age 20–73 years, mean 29.7), see details below.

This data was used for axon diameter distribution (ADD) demonstration in specific tracts as well as for estimating the diffusion protocol effect on ADD values along the corpus callosum (CC).

Subject were scanned on a 3T Magnetom Siemens Prisma (Siemens, Erlangen, Germany) scanner with a 64-channel RF coil and a gradient system reaching 80mT/m. The scans include the following sequences:

1. A multi-shell diffusion-weighted imaging (DWI) sequence, with the parameters detailed in Table 1 (two protocol versions).
2. An MPRAGE sequence, with the parameters detailed in Table 2.

Table 1
Experimental parameters for diffusion scans.

Protocol	TR/TE [ms]	Bval [s/mm^2]	#Dir	maxG [G/cm]	Δ/δ [ms]	#Voxels	Resolution [mm^3]
1	5200/118	0, 250, 1000, 3000 & 5000	88	7.2	60/15.5	120x120x90	1.7x1.7x1.7
2	3500/94	0, 1000, 2000 & 4000	186	7.9	45/15	128x128x88	1.6x1.6x1.6

Table 2
Experimental parameters for MPRAGE scans.

TR/TE [ms]	TI [ms]	#Voxels	Resolution [mm^3]
2400/2.78	1000	224x224x160	1x1x1

For group analysis of ADD, we used scans from the HCP database. We used multi-shell DWI scans and high quality T1w structural images data for randomly selected healthy adults (324 subjects: 180 females, age 22–37, mean 28.9) from HCP 1200 young adults release [63]. A subset (22 subjects: 13 females, age 22–35 years, mean 28.9) was used for analysis of the diffusion protocol effect on ADD values along the CC. Full protocol details available in the HCP reference manual (https://www.humanconnectome.org/storage/app/media/documentation/s1200/HCP_S1200_Release_Reference_Manual.pdf)

All experiments were performed in accordance with the Declaration of Helsinki. The imaging protocol was approved by the institutional review boards of Sheba Medical Centers and Tel Aviv University, where the MRI investigations were performed. All subjects provided signed informed consent before enrollment in the study.

Preprocessing

The TAU Brain Bank scans preprocessing pipeline includes top-up and eddy corrections, as well as registration of MPRAGE to diffusion image using the Functional MRI of the Brain (FMRIB) linear image registration tool [64, 65]. The HCP provides minimally preprocessed images [66]. This preprocessing pipeline includes intensity normalization across runs, top-up and eddy corrections, gradient nonlinear correction, and registration of MPRAGE to diffusion image using the Functional MRI of the Brain (FMRIB) linear image registration tool boundary-based registration. The full pipeline is available online (https://github.com/Washington-University/Pipelines). Furthermore, all HCP scans were registered to MNI space for group analysis of the ADD maps, using the FMRIB non-linear image registration tool [67].

Diffusion-based tractography

The Fiber tracking analysis for TAU Brain Bank scans was conducted using a pipeline of multi-shell multi-tissue CSD reconstruction with Continuous Map Criterion (CMC) stopping criterion that accounts for partial volumes, based on the DiPy Library [68]. The Fiber tracking analysis for HCP scans was conducted using the Mrtrix3 software package [69], which uses a multi-tissue spherical convolution model that accounts for partial volumes [70].

Weighting streamlines

The AxSI framework resulted in a 3D image, while the value in each voxel represents the eMAD resulting from the analysis. After reconstructing streamlines from the entire brain, each streamline was weighted by the average eMAD value of all the voxels it passed through.

Network matrices

Based on AxSI analysis results and whole brain tractography, we calculated the weighted network matrices of each subject, while the nodes were defined as the Brainnetome Atlas areas [71], which was built upon a connectivity-based parcellation framework. The edges were weighted as the average of ADD of all streamlines connected two brain areas, after a non-linear registration of the atlas to the subject's diffusion scan space.

Fascicle extraction

CC bundles were extracted using a 2D midsagittal CC mask for each subject. The masks were created using automatic region-of-interest selection based on FA map intensity and then manually checked and corrected based on the T1 scans where necessary. We then filtered the full brain tracts to only include tracts passing through the corpus callosum mask. The extraction of Corona Radiata (CR), Inferior Fronto-Occipital Fasciculus (IFOF), and Superior Longitudinal Fasciculus (SLF) tracts, has been conducted manually, using ROI masks, for a single subject from the TAU Brain Bank for demonstration.

Surface representations of average ADD

Network matrices weighted by the average ADD were calculated as described above. We then calculated the mean weight of each edge over the entire group of HCP subjects (excluding zeros from calculation) to create a weighted network matrix of the group. We used Median Absolute Deviation (MAD) outlier detection for each edge, in order to exclude extreme values [72].

The group matrix was used to calculate the average ADD arriving at each node in the average weighted network. In the surface representation of the mean ADD weighted brain areas, each area value is a representation of the mean value of ADD of streamlines arriving at it in the averaged network.

Average ADD maps

To create the average ADD WM maps, we first created an ADD WM map for each subject, by calculating the average of ADD values of all streamlines that pass through each voxel. We then registered all maps to MNI space, as described in the preprocessing section. Finally, we calculated the average value for each voxel and masked the resulting map using a WM mask of the MNI template brain. Values of ADD < 0.3um were excluded from calculation to reduce the noise derived from very small ADD related signal.

Statistics

The AxSI analysis values were used to compare between the estimated ADD of each CC section for three different scan protocols. Repeated-measures ANOVA was used for comparisons between the five callosal sections which were segmented according to Witelson's parcellation [73].

Declarations

Acknowledgments

Funding

Israel Science Foundation 1303/20 (YA)

BIRAX, British Council 43BX-PO:4503275594 (YA)

NSFBSF 2018711 (YA)

Author contributions

Software: HG, AH, YA

Resources: RK, DB

Data Curation: DB

Methodology: HG, AH, DB, SL, SBA, YA

Investigation: HG, AH, DB, SBA, YA

Visualization: HG, YA

Supervision: YA

Writing—original draft: HG, YA

Writing—review & editing: HG, YA

Competing interests

Authors declare that they have no competing interests.

Data and materials availability

All code and averaged results are available in the main text or the supplementary materials.

All data are available upon reasonable request

References

1. A. K. Engel, C. K. Moll, I. Fried, G. A. Ojemann, Invasive recordings from the human brain: clinical insights and beyond. Nat Rev Neurosci **6**, 35–47 (2005).
2. J. Parvizi, S. Kastner, Promises and limitations of human intracranial electroencephalography. Nat Neurosci **21**, 474–483 (2018).
3. A. W. Toga, *Brain Mapping: An Encyclopedic Reference*. (Elsevier Science & Technology, San Diego, United States, 2015).
4. H. S. Gasser, H. Grundfest, Axon diameters in relation to the spike dimensions and the conduction velocity in mammalian a fibers. Am J Physiol **127**, 393–414 (1939).

5. L. Goldman, J. S. Albus, Computation of impulse conduction in myelinated fibers; theoretical basis of the velocity-diameter relation. Biophys J **8**, 596–607 (1968).
6. S. G. Waxman, Determinants of conduction velocity in myelinated nerve fibers. Muscle Nerve **3**, 141–150 (1980).
7. A. Horowitz *et al.*, In vivo correlation between axon diameter and conduction velocity in the human brain. Brain Struct Funct, (2014).
8. D. Barazany, P. J. Basser, Y. Assaf, In vivo measurement of axon diameter distribution in the corpus callosum of rat brain. Brain **132**, 1210–1220 (2009).
9. Y. Assaf, T. Blumenfeld-Katzir, Y. Yovel, P. J. Basser, AxCaliber: a method for measuring axon diameter distribution from diffusion MRI. Magn Reson Med **59**, 1347–1354 (2008).
10. Y. Assaf *et al.*, The CONNECT project: Combining macro- and micro-structure. Neuroimage **80**, 273–282 (2013).
11. Y. Assaf, H. Johansen-Berg, M. Thiebaut de Schotten, The role of diffusion MRI in neuroscience. NMR Biomed **32**, e3762 (2019).
12. T. B. Dyrby, L. V. Sogaard, M. G. Hall, M. Ptito, D. C. Alexander, Contrast and stability of the axon diameter index from microstructure imaging with diffusion MRI. Magn Reson Med **70**, 711–721 (2013).
13. A. Daducci *et al.*, Accelerated Microstructure Imaging via Convex Optimization (AMICO) from diffusion MRI data. Neuroimage **105**, 32–44 (2015).
14. D. Romascano *et al.*, ActiveAxADD: Toward non-parametric and orientationally invariant axon diameter distribution mapping using PGSE. Magn Reson Med **83**, 2322–2330 (2020).
15. D. Barazany, D. Jones, Y. Assaf, AxCaliber 3D. Proc Intl Soc Magn Reson Med **19**, 76 (2011).
16. A. Daducci, A. Dal Palu, A. Lemkaddem, J. P. Thiran, COMMIT: Convex optimization modeling for microstructure informed tractography. IEEE Trans Med Imaging **34**, 246–257 (2015).
17. M. Barakovic *et al.*, Bundle-Specific Axon Diameter Index as a New Contrast to Differentiate White Matter Tracts. Front Neurosci **15**, 646034 (2021).
18. K. D. Harkins, C. Beaulieu, J. Xu, J. C. Gore, M. D. Does, A simple estimate of axon size with diffusion MRI. Neuroimage **227**, 117619 (2021).
19. J. Veraart *et al.*, Nonivasive quantification of axon radii using diffusion MRI. Elife **9**, (2020).
20. M. Drakesmith *et al.*, Estimating axon conduction velocity in vivo from microstructural MRI. Neuroimage **203**, 116186 (2019).
21. H. H. Lee *et al.*, Along-axon diameter variation and axonal orientation dispersion revealed with 3D electron microscopy: implications for quantifying brain white matter microstructure with histology and diffusion MRI. Brain Struct Funct **224**, 1469–1488 (2019).
22. F. Sepehrband, D. C. Alexander, N. D. Kurniawan, D. C. Reutens, Z. Yang, Towards higher sensitivity and stability of axon diameter estimation with diffusion-weighted MRI. NMR Biomed **29**, 293–308 (2016).
23. S. Y. Huang *et al.*, High-gradient diffusion MRI reveals distinct estimates of axon diameter index within different white matter tracts in the in vivo human brain. Brain Struct Funct **225**, 1277–1291 (2020).
24. S. Y. Huang *et al.*, The impact of gradient strength on in vivo diffusion MRI estimates of axon diameter. Neuroimage **106**, 464–472 (2015).
25. C. Beaulieu, The basis of anisotropic water diffusion in the nervous system - a technical review. NMR Biomed **15**, 435–455 (2002).
26. C. Beaulieu, F. R. Fenrich, P. S. Allen, Multicomponent water proton transverse relaxation and T2-discriminated water diffusion in myelinated and nonmyelinated nerve. Magn Reson Imaging **16**, 1201–1210 (1998).
27. Y. Assaf, Y. Cohen, Non-mono-exponential attenuation of water and N-acetyl aspartate signals due to diffusion in brain tissue. J Magn Reson **131**, 69–85 (1998).

28. Y. Assaf, Y. Cohen, Assignment of the water slow-diffusing component in the central nervous system using q-space diffusion MRS: implications for fiber tract imaging. Magn Reson Med **43**, 191–199 (2000).
29. E. Fieremans *et al.*, In vivo observation and biophysical interpretation of time-dependent diffusion in human white matter. Neuroimage **129**, 414–427 (2016).
30. H. H. Lee, E. Fieremans, D. S. Novikov, What dominates the time dependence of diffusion transverse to axons: Intra- or extra-axonal water? Neuroimage **182**, 500–510 (2018).
31. Y. Assaf *et al.*, Changes in axonal morphology in experimental autoimmune neuritis as studied by high b-value q-space (1)H and (2)H DQF diffusion magnetic resonance spectroscopy. Magn Reson Med **48**, 71–81 (2002).
32. S. Peled, D. G. Cory, S. A. Raymond, D. A. Kirschner, F. A. Jolesz, Water diffusion, T(2), and compartmentation in frog sciatic nerve. Magn Reson Med **42**, 911–918 (1999).
33. G. J. Stanisz, R. M. Henkelman, Diffusional anisotropy of T2 components in bovine optic nerve. Magn Reson Med **40**, 405–410 (1998).
34. G. J. Stanisz, A. Szafer, G. A. Wright, R. M. Henkelman, An analytical model of restricted diffusion in bovine optic nerve. Magn Reson Med **37**, 103–111 (1997).
35. J. Veraart, E. P. Raven, L. J. Edwards, N. Weiskopf, D. K. Jones, The variability of MR axon radii estimates in the human white matter. Hum Brain Mapp **42**, 2201–2213 (2021).
36. M. Paquette, C. Eichner, T. R. Knoesche, A. A., Axon Diameter Measurements using Diffusion MRI are Infeasible. *bioRxiv*, (2021).
37. Y. Assaf, P. J. Basser, Composite hindered and restricted model of diffusion (CHARMED) MR imaging of the human brain. Neuroimage **27**, 48–58 (2005).
38. Y. Assaf, R. Z. Freidlin, G. K. Rohde, P. J. Basser, New modeling and experimental framework to characterize hindered and restricted water diffusion in brain white matter. Magn Reson Med **52**, 965–978 (2004).
39. D. K. Jones, *Diffusion MRI: theory, methods, and application*. (Oxford University Press, New York, 2010), pp. xvi, 767 p.
40. P. van Gelderen, D. DesPres, P. C. van Zijl, C. T. Moonen, Evaluation of restricted diffusion in cylinders. Phosphocreatine in rabbit leg muscle. J Magn Reson B **103**, 255–260 (1994).
41. F. Aboitiz, A. B. Scheibel, R. S. Fisher, E. Zaidel, Fiber composition of the human corpus callosum. Brain Res **598**, 143–153 (1992).
42. S. Tomasi, R. Caminiti, G. M. Innocenti, Areal differences in diameter and length of corticofugal projections. Cereb Cortex **22**, 1463–1472 (2012).
43. Y. Suzuki *et al.*, Estimation of the Mean Axon Diameter and Intra-axonal Space Volume Fraction of the Human Corpus Callosum: Diffusion q-space Imaging with Low q-values. Magn Reson Med Sci **15**, 83–93 (2016).
44. J. A. McNab *et al.*, in *Int. Soc. Magn. Reson. Med.* (Melbourne, Australia, 2012), vol. 19, pp. 1530.
45. D. S. Novikov, V. G. Kiselev, S. N. Jespersen, On modeling. Magn Reson Med **79**, 3172–3193 (2018).
46. J. Brabec, S. Lasic, M. Nilsson, Time-dependent diffusion in undulating thin fibers: Impact on axon diameter estimation. NMR Biomed **33**, e4187 (2020).
47. M. Nilsson, D. van Westen, F. Stahlberg, P. C. Sundgren, J. Latt, The role of tissue microstructure and water exchange in biophysical modelling of diffusion in white matter. MAGMA **26**, 345–370 (2013).
48. G. Zhu *et al.*, Applications of Deep Learning to Neuro-Imaging Techniques. Front Neurol **10**, 869 (2019).
49. D. Ma *et al.*, Magnetic resonance fingerprinting. Nature **495**, 187–192 (2013).
50. I. Tavor *et al.*, Task-free MRI predicts individual differences in brain activity during task performance. Science **352**, 216–220 (2016).
51. M. F. Glasser, D. C. Van Essen, Mapping human cortical areas in vivo based on myelin content as revealed by T1- and T2-weighted MRI. J Neurosci **31**, 11597–11616 (2011).

52. D. Liewald, R. Miller, N. Logothetis, H. J. Wagner, A. Schuz, Distribution of axon diameters in cortical white matter: an electron-microscopic study on three human brains and a macaque. Biol Cybern **108**, 541–557 (2014).
53. R. Olivares, S. Michalland, F. Aboitiz, Cross-species and intraspecies morphometric analysis of the corpus callosum. Brain Behav Evol **55**, 37–43 (2000).
54. D. S. Bassett, O. Sporns, Network neuroscience. Nat Neurosci **20**, 353–364 (2017).
55. O. Sporns, *Networks of the brain*. (MIT Press, Cambridge, Mass., 2011), pp. xi, 412 p., 418 p. of plates.
56. J. A. McNab *et al.*, in *Organization of Human Brain Mapping*. (Beijing, China, 2012), pp. 665.
57. D. S. Novikov, E. Fieremans, S. N. Jespersen, V. G. Kiselev, Quantifying brain microstructure with diffusion MRI: Theory and parameter estimation. NMR Biomed **32**, e3998 (2019).
58. P. T. Callaghan, *Principles of nuclear magnetic resonance microscopy*. (Clarendon Press; New York : Oxford University Press, Oxford, 1991).
59. S. Lasic, M. Nilsson, J. Latt, F. Stahlberg, D. Topgaard, Apparent exchange rate mapping with diffusion MRI. Magn Reson Med **66**, 356–365 (2011).
60. A. L. Busza *et al.*, Diffusion-weighted imaging studies of cerebral ischemia in gerbils. Potential relevance to energy failure. Stroke **23**, 1602–1612 (1992).
61. L. Brusini, G. Menegaz, M. Nilsson, Monte Carlo Simulations of Water Exchange Through Myelin Wraps: Implications for Diffusion MRI. IEEE Trans Med Imaging **38**, 1438–1445 (2019).
62. A. Horowitz *et al.*, In vivo correlation between axon diameter and conduction velocity in the human brain. Brain Struct Funct **220**, 1777–1788 (2015).
63. D. C. Van Essen *et al.*, The WU-Minn Human Connectome Project: an overview. Neuroimage **80**, 62–79 (2013).
64. M. Jenkinson, S. Smith, A global optimisation method for robust affine registration of brain images. Med Image Anal **5**, 143–156 (2001).
65. M. Jenkinson, P. Bannister, M. Brady, S. Smith, Improved optimization for the robust and accurate linear registration and motion correction of brain images. Neuroimage **17**, 825–841 (2002).
66. M. F. Glasser *et al.*, The minimal preprocessing pipelines for the Human Connectome Project. Neuroimage **80**, 105–124 (2013).
67. J. L. R. Andersson, M. Jenkinson, S. A. Smith, "Non-linear registration aka Spatial normalisation," *FMRIB Technial Report TR07JA2* (FMRIB, Oxford, United Kingdom, 2007).
68. E. Garyfallidis *et al.*, Dipy, a library for the analysis of diffusion MRI data. Front Neuroinform **8**, 8 (2014).
69. J. D. Tournier *et al.*, MRtrix3: A fast, flexible and open software framework for medical image processing and visualisation. Neuroimage **202**, 116137 (2019).
70. R. Krupnik, Y. Yovel, Y. Assaf, Inner- and inter- hemispheric connectivity balance in the human brain. *J neurosci* **Accepted**, (2021).
71. L. Fan *et al.*, The Human Brainnetome Atlas: A New Brain Atlas Based on Connectional Architecture. Cereb Cortex **26**, 3508–3526 (2016).
72. C. Leys, C. Ley, O. Klein, B. P., L. Licata, Detecting outliers: Do not use standard deviation around the mean, use absolute deviation around the median. Journal of Experimental Social Psychology **49**, 764–766 (2013).
73. S. F. Witelson, Hand and sex differences in the isthmus and genu of the human corpus callosum. A postmortem morphological study. Brain **112** (**Pt 3**), 799–835 (1989).
74. Abdollahzadeh, A., Belevich, I., Jokitalo, E., Tohka, J., & Sierra, A., Automated 3D axonal morphometry of white matter. Scientific reports, *9*(1), 1–16 (2019).
75. Virtanen, J., Uusitalo, H., Palkama, A., & Kaufman, H., The effect of fixation on corneal endothelial cell dimensions and morphology in scanning electron microscopy. Acta Ophthalmol (Copenh), **62**(4), 577-585 (1984).

76. Beaulieu, C., Fenrich, F. R., & Allen, P. S., Multicomponent water proton transverse relaxation and T2-discriminated water diffusion in myelinated and nonmyelinated nerve. Magnetic resonance imaging, **16**(10), 1201–1210 (1998).
77. Beaulieu, C., The basis of anisotropic water diffusion in the nervous system–a technical review. NMR in Biomedicine: An International Journal Devoted to the Development and Application of Magnetic Resonance In Vivo, **15**(7-8), 435–455 (2002).

Figures

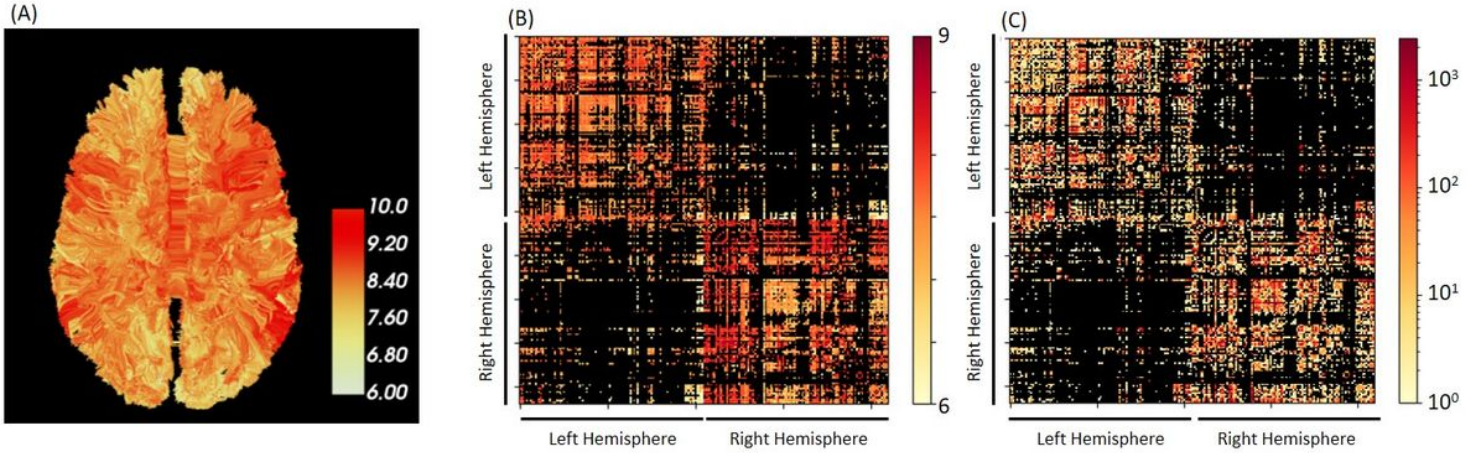

Figure 1

ADD weighted Connectome. (**A**) Whole brain tractography of a single subject, weighted by the average ADD. (**B**) Network matrix representation of the same subject, weighted by the average ADD of streamlines that connect each pair of brain regions. (**C**) Network matrix representation of the same subject, weighted by the number of streamlines that connect each pair of brain regions.

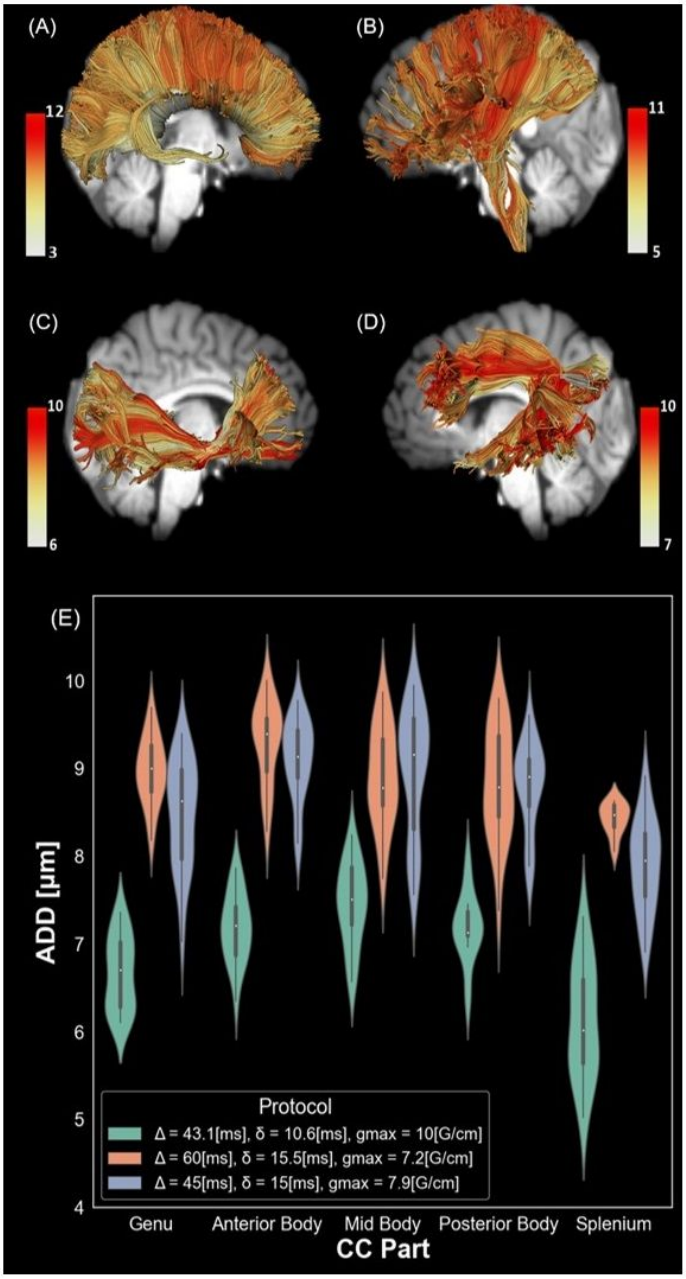

Figure 2

EMAD values resulting from AxSI analysis. (**A-D**) Visual representations of the eMAD distribution in the CC (**A**), CR (**B**), IFOF (**C**) & SLF (**D**) bundles from AxSI analysis of a single human subject. Different colors represent different estimations of ADD (in µm, see colorbars). (**E**) Violin plots for the estimated axon diameter in different parts of the CC, for three different protocols (see Methods). White point represents the median value, mini-box for quartiles and the violin is a kernel density estimation of the underlying distribution

Figure 3

Axon diameter weighted cortical surface representation. The figure shows the average eMAD value of all streamlines connected to each brain region from the Brainnetome Atlas, from four different points of view. Darker color (redder) represents higher values (in μm, see colorbar).

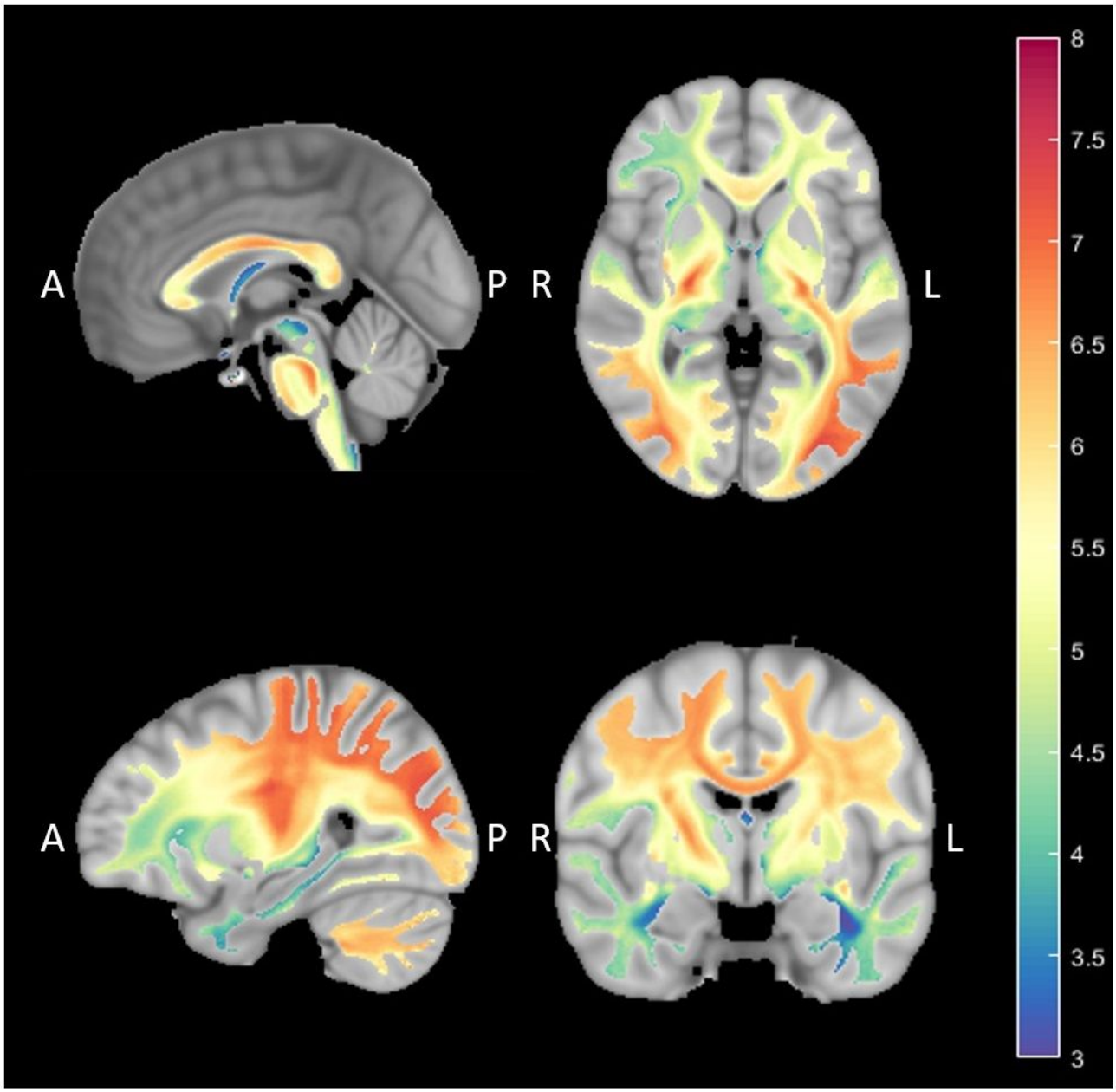

Figure 4

Average axon diameter WM reference map. Highlight slices from the resulting map demonstrate interesting characteristics of axon diameter distribution in the WM as resulted from a group analysis of HCP data. Colors represent voxel-based averaging eMAD for subjects' maps after registration to MNI space (in μm, see colorbar).

Supplementary Files

This is a list of supplementary files associated with this preprint. Click to download.

- AxonalSpectrumImagingScientificReportsSupplementary.pdf